NANOSYSTEMS: PHYSICS, CHEMISTRY, MATHEMATICS, 2014, 5 (4), P. 553–563

# SYNTHESIS AND PHOTOCATALYTIC ACTIVITY OF QUASI-ONE-DIMENSIONAL (1-D) SOLID SOLUTIONS $Ti_{1-x}M_xO_{2-2x/2}$ (M(III)= Fe(III), Ce(III), Er(III), Tb(III), Eu(III), Nd(III) and Sm(III), $0 \leq x \leq 0.1$)

E. V. Polyakov, V. N. Krasilnikov, O. I. Gyrdasova, L. Yu. Buldakova, M. Yu. Yanchenko

Institute of Solid State Chemistry UB RAS, str. Pervomajskaya, 91,
620990,Ekaterinburg, Russia

Polyakov@ihim.uran.ru, tel.: +7 343 3744814, fax.: +7 343 3744495

**PACS 82.33.Pt, 82.50.-m**

Quasi-one-dimensional (1–D) solid solutions $Ti_{1-x}M_xO_{2-x/2}$ (M(III)=Fe(III), Ce(III), Er(III), Tb(III), Eu(III), Nd(III), Sm(III), $0 < x \leq 0.1$) with the anatase structure have been synthesized by heating glycolate $Ti_{1-x}M_x(OCH_2CH_2O)_{2-x/2}$ in air at a temperature above 450 °C. A method was proposed for the production of iron-and carbon-doped titanium dioxide with the anatase structure $Ti_{1-x}Fe_xO_{(2-x/2)-y}C_y$ and of composites based thereon containing an excessive carbon content. It was shown that the oxide solid solutions exhibit photocatalytic activity in the hydroquinone photooxidation reaction during irradiation in the ultraviolet spectrum. A correlation was established between the hydroquinone oxidation rate and the concentration of the substituting ions 'M' in the catalyst. In the framework of the theory of ion-covalent binary solid solutions, a correlation was found between the energy of the photocatalytic reaction and the estimated mixing enthalpy of binary solid solutions formation.

**Keywords:** glycolates, three-charged cations, anatase, synthesis, photocatalytic properties.

*Received: 16 June 2014*
*Revised: 30 June 2014*

## 1. Introduction

Titanium oxides are the basis of advanced ceramics, pigments, membranes, sorbents, phosphors, and catalysts, including materials for direct decomposition of water under exposure to light and for photocatalytic oxidation of organic substances [1]. The drawback of powdered titanium oxide as a photocatalyst is its relatively high recombination rate of electron-hole pairs and consequently a low quantum yield for photooxidation. Improvement of photocatalytic properties of $TiO_2$ and its derivative composites is an important problem of materials science since these are environmentally-friendly and easily-produced materials. The activity of $TiO_2$-based photocatalysts depends on the acid-base properties of materials, the morphology of constituent particles, and on the nature of the photocatalytic reactions [2, 3]. Attempts to enhance the photocatalytic characteristics of $TiO_2$ were directed at controlling its phase composition by temperature treatment, doping with transition metal or non-metal ions, or by modification of the bulk and surface properties of titania by semiconducting phases of other oxide compounds or coloring agents to improve the spectral properties of the photocatalyst [1–18]. Recently, numerous studies of nano-sized extended (quasi-one-dimensional) morphological analogues of powdered titanium oxide (wires, whiskers, tubes) were performed. Theoretical analysis of the electronic structure of quasi-one-dimensional titanium oxides predicts that unusual catalytic properties can appear for these materials as a result of varying their morphology and chemical composition [1–11]. These

approaches for shifting the oxides' photoactivity from the typical ultraviolet spectrum to the visible region holds a special place in the investigations of quasi-one-dimensional titanium oxides. An efficient method for the synthesis of nanodispersed quasi-one-dimensional $TiO_2$ is the so-called precursor technique, based on pseudomorphic transformation of the precursor into oxide during heating [12–15]. A bathochromic shift of photocatalytic activity of titanium dioxide from the ultraviolet to visible spectrum is the main objective of titania doping with d-, f-elements, halogens, boron, carbon, nitrogen, bismuth, and sulfur [2, 16–21]. For example, these problems were comprehensively solved by employing the glycolate $Ti_{1-x}V_x(OCH_2CH_2O)_2$ as a precursor of doped titania. Namely, a quasi-one-dimensional anatase of the compositions $Ti_{1-x}V_xO_2$ and $Ti_{1-x}V_xO_{2-y}C_y$ was synthesized, which has a high photocatalytic activity in the oxidation of hydroquinone in an aqueous solution during irradiation both in the ultraviolet and visible (blue) regions [22, 23]. Solid solutions of the compositions $Ti_{1-x}Ce_xO_2$ and $Ti_{1-x}Ln_xO_{2-x/2}$, where Ln is Nd, Sm, Eu, Tb, Er or Yb, having aggregates of different morphology [24, 25], have been also synthesized by thermolysis of $Ti_{1-x}Ln_x(OCH_2CH_2O)_{2-x/2}$, but the anticipated high activity of $Ti_{1-x}Ln_xO_{2-x/2}$ in the photocatalytic oxidation of hydroquinone was not reached. In contrast, it was reported [3, 19, 25, 26] that the introduction of Fe(III) cations into the structure of $TiO_2$ grains can increase its catalytic activity in the photooxidation of toxic organic compounds and even shift it into the visible region. At the same time, no data on the synthesis and photocatalytic activity of quasi-one-dimensional (1-D) iron-doped titanium dioxide are available in the literature. Therefore, the main aims of our work were the preparation of elongated fibers of Fe(III)-doped titanium dioxide $Ti_{1-x}Fe_xO_{2-x/2}$ and comparison of its photocatalytic activity with that of morphologically similar lanthanide-substituted solid solutions in the titanium oxide phase using the hydroquinone oxidation reaction in water as an example, as well as elucidation of the reasons for the change of the catalytic activity of titanium oxides in the series of tricharged doped cations.

## 2. Experimental

### 2.1. Materials and Synthesis

All the reagents were analytically pure and were used in the experiment without further purification.

$Ti_{1-x}Fe_xO_{2-x/2}$ was synthesized by the precursor method [14, 15] using the glycolate $Ti_{1-x}Fe_x(OCH_2CH_2O)_{2-x/2}$ as a precursor, which was produced in the reaction:

$$(1-x)Ti(OH)_4 + xFe(OH)_3 + (2-x/2)HOCH_2CH_2O = Ti_{1-x}Fe_x(OCH_2CH_2O)_{2-x/2} + (4-x/2)H_2O. \quad (1)$$

Ti(IV) and Fe(III) hydroxides required for reaction (1) were obtained by co-precipitation from aqueous solutions $TiOSO_4 \cdot 2H_2O$ and $Fe_2(SO_4)_3 \cdot 9H_2O$ (p.a.) with addition of an aqeous solution of ammonia to pH 7.5 to 8. The precipitates were washed with distilled water until a negative reaction to $SO_4^{2-}$ ions was reached both in rinsing water and in the precipitates, then they were partially dehydrated on a vacuum filter and were mixed with ethylene glycol (p.a.) in a molar ratio $Ti(OH)_4$, $Fe(OH)_3/HOCH_2CH_2OH = 1/50$. The resulting mixtures were heated in 250 ml heat-resistant cone flasks at temperatures below the ethylene glycol boiling point (197.6 °C) for 2 to 5 h. Since ethylene glycol was used simultaneously as a reactant and a reaction medium, it was taken in excess with respect to reaction (1) of the titanium and iron hydroxides transformation. $Ti_{1-x}Fe_x(OCH_2CH_2O)_{2-x/2}$ precipitate was crystallized in a supersaturated solution by evaporation of excess ethylene glycol. The resulting precipitates

$Ti_{1-x}Fe_x(OCH_2CH_2O)_{2-x/2}$ were separated from excessive unreacted ethylene glycol by vacuum filtration, then were washed with acetone and dried at a temperature of about 50 °C to remove residual acetone. Finally, they were placed into airtight weighing bottles for storage. In order to compare the effect of tricharged cations on the photocatalytic properties of doped titania, we have synthesized the samples of glycolates of some rare-earth elements with a fixed concentration of the dopant, $Ti_{1-x}Ln_x(OCH_2CH_2O)_{2-x/2}$, where Ln is Nd, Sm, Eu, Tb, or Er and $x = 0.025$. In addition, the cerium-substituted glycolate $Ti_{1-x}Ce_x(OCH_2CH_2O)_{2-x/2}$ ($x = 0.05, 0.1, 0.2$ and $0.3$) was synthesized.

## 2.2. Characterization

Phase analysis of the synthesized samples was performed with a POLARAM S-112 polarized microscope in transmitted light and a STADI-P (STOE, Germany) X-ray diffractometer in CuK$\alpha$ radiation; thermogravimetric analysis was carried out using a Setaram SetsysEvolution thermal analyzer during heating in air at a rate of 10 °C/min. The form and shape of the precursor particles and the products of their thermolysis were determined by the scanning electron microscopy method on a JSM JEOL 6390LA device. Elemental analysis of the examined samples for titanium and iron content was performed by the atomic adsorption spectroscopy method in an air-acetylene flame on a Perkin-Elmer device and by atomic emission technique on a inductive-plasma spectrum analyzer. The content of carbon was determined according to the technique described in detail in work [22]. IR spectra of the powders were registered on a Spectrum–One spectrometer (Perkin-Elmer from 4000 to 400 $cm^{-1}$. The solutions were irradiated in 50 ml quartz cells with a UV-BUF-15 lamp ($\lambda_{max} = 253$ nm); for irradiation in the visible spectrum, we used a blue luminescent lamp with maximum irradiation from 440–460 nm.

## 2.3. Photocatalytic experiments

The photocatalytic activities of the $Ti_{1-x}Fe_xO_{2-x/2}$ and $Ti_{1-x}Ln_xO_{2-x/2}$ catalyst samples were examined in terms of hydroquinone (substrate, HQ) solution decomposition. In a typical experiment, 100 mg of the catalyst were magnetically stirred in a 50 ml 0.10 mmol/l HQ solution in darkness for 1 hr in order to achieve the adsorption–desorption equilibrium between HQ and the catalyst. The suspension of the catalyst in the solution was then irradiated with an ultraviolet light using a BUF 15 lamp ($\lambda_{max} = 253$ nm) during assigned exposure time from zero to one hour. The level of photocatalytic decomposition of the substrate was evaluated using current–voltage characteristics [22]. Preliminary sorption experiments in the system 'catalyst – HQ' at different HQ concentrations and different masses of the catalyst have showed that the distribution of HQ between the solution and the catalysts obeys the Langmuir's law. Thus, the selected initial concentration of HQ in the photocatalytic experiments allowed us to carry out HQ sorption and photocatalysis within the Henry's law region $< 0.4$ mM.

Quantitative variation of the HQ concentration in the solution during photocatalytic oxidation in the presence of $Ti_{1-x}Fe_xO_{2-x/2}$ and $Ti_{1-x}Ln_xO_{2-x/2}$ catalysts was estimated by the voltammetry method on a PU-1 polarograph with the rate of potential scanning of 0.03 V/s [22, 23]. The PU-1 polarograph was coupled with a cylindrical carbon indicator electrode with working surface area of 0.44 $cm^2$ and with an additional AgCl-electrode EVL-1M3. The substrate concentration was determined at the cathode potential of $-0.5$ V. Anode polarization of the electrodes in the region 0.0–1.0 V was used every time after cathode polarization to purify the electrode surface.

## 3. Results and discussions

### 3.1. Characterization of catalysts

According to X-ray phase, microscopic analyses and IR spectroscopy data, the products of reaction (1) are found to be solid solutions of the composition $Ti_{1-x}Fe_x(OCH_2CH_2O)_{2-x/2}$ ($0 < x \leq 0.1$) formed by substitution of Fe(III) for Ti(IV) in the structure of titanium glycolate $Ti(OCH_2CH_2O)_2$. Depending on the reaction conditions and quantitative ratios of reagents, they can be produced as extended $0.5 - 2 \times 5 - 20$ $\mu$m crystalline fibers of approximately the same length with cross-sections of about 50–100 nm. Most thin fibrous crystals $Ti_{1-x}Fe_x(OCH_2CH_2O)_{2-x/2}$ are formed during slow evaporation of the solvent — ethylene glycol from its saturated solutions. However, the glycolate crystals formed at the initial stage of evaporation tend to display longitudinal intergrowth, which leads to the formation of aggregates with the cross-section greater than 0.5 $\mu$m. Depending on the content of iron, the color of $Ti_{1-x}Fe_x(OCH_2CH_2O)_{2-x/2}$ powders varies from pale yellow ($x \leq 0.05$) to orange ($0.05 < x \leq 0.1$). Close similarity of IR spectra for $Ti(OCH_2CH_2O)_2$ and $Ti_{1-x}Fe_x(OCH_2CH_2O)_{2-x/2}$ at $x \leq 0.1$ is indicative of a small distortion of the initial crystal structure of the titanium glycolate as a result of the substitution of Fe(III) for Ti(IV) cations. The same similarity is typical of the IR spectra of $Ti_{1-x}V_x(OCH_2CH_2O)_2$ [14,22] and $Ti_{1-x}Ln_x(OCH_2CH_2O)_{2-x/2}$ [24], which implies a similar nature of the solid solutions based on titanium glycolate $Ti(OCH_2CH_2O)_2$. A very intense band at 1058 cm$^{-1}$ corresponds to vibrations of bonds C–O– in the metal-coordinated bis-alkoxide ion $OCH_2CH_2O^{2-}$ in the IR spectra of $Ti_{0.9}Fe_{0.1}(OCH_2CH_2O)_{1.95}$ and $Ti(OCH_2CH_2O)_2$, while in the spectrum of liquid ethylene glycol two bands of the same intensity are present in this region at 1087 and 1043 cm$^{-1}$ [27]. Intense absorption bands with maxima at 918 and 880 cm$^{-1}$ displaced to the high-frequency region relative to those in the IR spectrum of liquid ethylene glycol (883 and 862 cm$^{-1}$) are attributed to torsional vibrations of the C–C bonds.

Aggregates of $Ti_{1-x}Fe_xO_{2-x/2}$ solid solutions, formed by heating the $Ti_{1-x}Fe_x(OCH_2CH_2O)_{2-x/2}$ precursor at 500 °C in air, have a morphology of elongated fiber-like aggregated particles. At low iron concentrations ($0.005 \leq x \leq 0.025$), the cross-section of these $Ti_{1-x}Fe_xO_{2-x/2}$ fibers is 50 to 100 nm, but as the concentration of Fe(III) increases, the thickness of the fibers increases (Fig. 1), obeying the tendency of primary precursor crystals to display intergrowth. Consequently, the thermal decomposition of $Ti_{1-x}Fe_x(OCH_2CH_2O)_{2-x/2}$ during heating in air to 500 °C gives rise to solid solutions which are pseudo-isomorphous to the precursor. The synthesized oxide $Ti_{1-x}Fe_xO_{2-x/2}$ fibers inherit the shape and morphology of the precursor fibrous crystals. We see that the shape of the $Ti_{1-x}Fe_xO_{2-x/2}$ oxide does not depend on the precursor thermal treatment conditions and remains unchanged upon heating in air or in an inert gaseous atmosphere up to 1300 °C. Moreover, it does not change as a result of the phase transformation of anatase to rutile, whose initial temperature exhibits a complicated dependence on the content of iron in $Ti_{1-x}Fe_xO_{2-x/2}$. Here we observe the following regularity: in the series of $Ti_{1-x}Fe_xO_{2-x/2}$ samples, the anatase to rutile phase transition onset temperature increases for $x < 0.05$ and decreases for $0.05 \leq x \leq 0.1$. Heating of $Ti_{0.95}Fe_{0.05}(OCH_2CH_2O)_{1.975}$ samples in air at 500 to 600 °C for 2 hr shows that the anatase to rutile phase transition in the resulting oxide $Ti_{0.95}Fe_{0.05}O_{1.97}$ begins at 550 °C. At the same time, for the product of thermolysis of $Ti_{0.9}Fe_{0.1}(OCH_2CH_2O)_{1.95}$, a phase with the rutile structure is observed already at 450 °C (Fig. 2). The products of thermolysis of $Ti_{1-x}Fe_x(OCH_2CH_2O)_{2-x/2}$ in helium atmosphere are black fibers, whose X-ray diffraction patterns contain very broad lines belonging to iron-doped titania with the anatase structure. The black color of the powders is due to the presence of

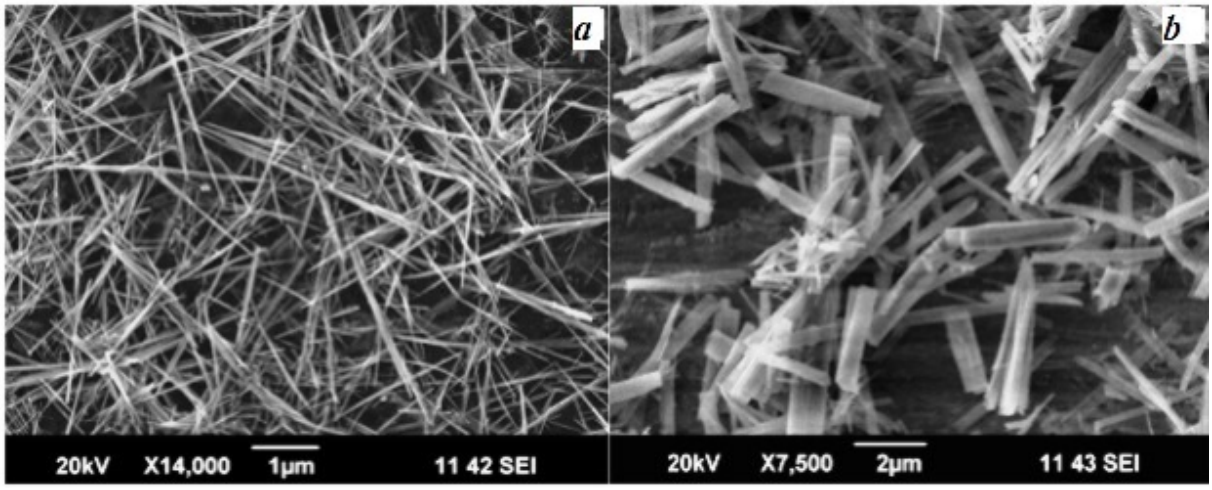


FIG. 1. SEM images of $Ti_{1-x}Fe_xO_{2-x/2}$ aggregates (a — $x = 0.01$, b — $x = 0.075$) obtained by heating of $Ti_{1-x}Fe_x(OCH_2CH_2O)_{2-x/2}$ in air at 500 °C

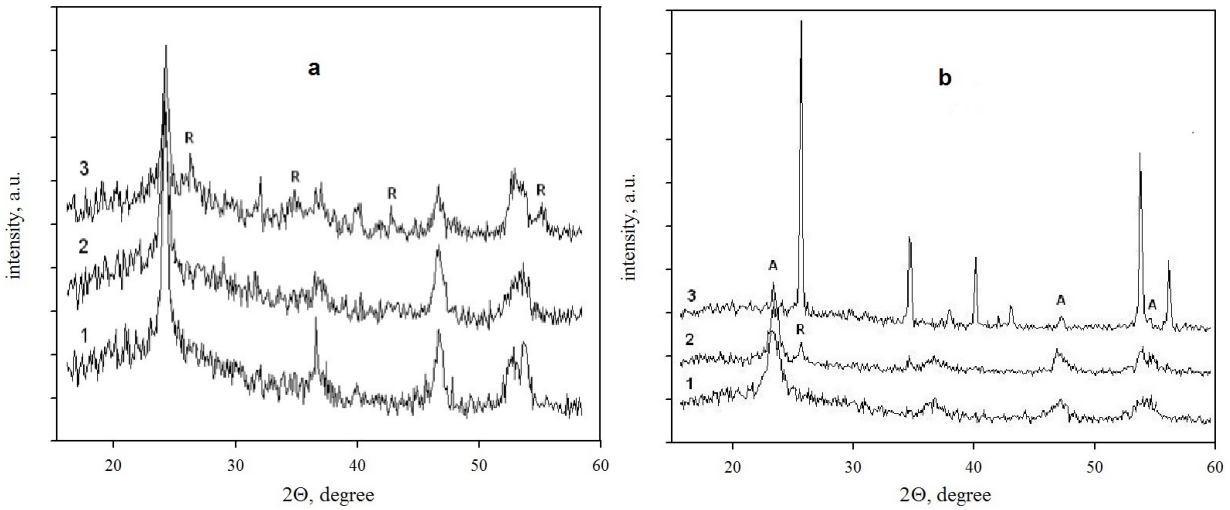


FIG. 2. a — X-ray diffraction patterns of thermolysis products of in air at 450 °C. 1 — $x = 0.025$, 2 — 0.05, 3 — 0.1. The tag 'R' denotes the lines of the rutile phase. b — X-ray diffraction patterns of thermolysis products of in helium atmosphere. 1 — 600, 2 — 800, and 3 — 900 °C. The tags 'R' and 'A' denote the lines of rutile and anatase phases

X-ray amorphous carbon: according to elemental and thermogravimetric (TG) analyses data, its content in all of the examined samples is about 18 mass %. Optical microscopy of the powders shows stretched black aggregates, which include both the anatase and black amorphous carbon particles. X-ray diffraction patterns of the $Ti_{0.95}Fe_{0.05}(OCH_2CH_2O)_{1.975}$ glycolate thermolysis products, which were heated for 2 hr in helium atmosphere to 600, 800,and 1000 °C, demonstrate high thermal stability of the anatase phase under an inert atmosphere. Even after 2 h exposure of the precursor at 1000 °C, the product contains an admixture of the phase with the anatase structure.

The TG and DTA curves of the glycolate $Ti_{0.95}Fe_{0.05}(OCH_2CH_2O)_{1.975}$ displayed in Fig. 3a show that the process of thermal decomposition of this material in air with a heating

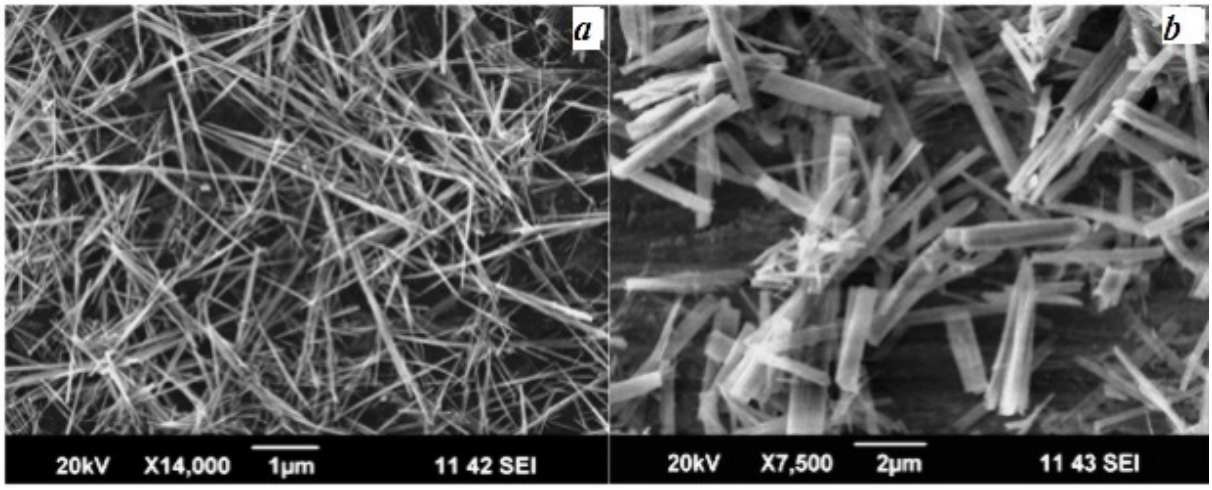


FIG. 3. a — TG and DTA curves of thermolysis product of $Ti_{0.95}Fe_{0.05}(OCH_2CH_2O)_{1.975}$ heated in air. b – TG and DTA curves of thermolysis product of $Ti_{0.95}Fe_{0.05}(OCH_2CH_2O)_{1.975}$ heated in helium atmosphere at 500 °C for 2 h.

rate of 10 °C/min has a complicated character and is exothermic from ∼ 250–500 °C with a maximum on the DTA curve at 315 °C. The mass loss value for the sample ($\Delta m = 52.33$ mass %) determined from the TG curve differs insignificantly from that ($\Delta m = 52.26$ mass %) calculated in the assumption that the oxide $Ti_{0.975}Fe_{0.025}O_{1.9875}$ is formed. The plateau on the TG curve in the temperature interval from ∼ 330 to 475 °C is due to the oxidation of X-ray amorphous carbon, formed as a result of redox decomposition of the glycolate ion $OCH_2CH_2O^{2-}$ at temperatures below 350 °C. The formation of carbon during the heating of $Ti_{1-x}Fe_x(OCH_2CH_2O)_{2-x/2}$ in air is confirmed by elemental analysis data, according to which, the samples exposed in air at 400 and 450 °C for 2 hr contain 1.2 and 0.58 mass % of structurally bound carbon, respectively. Fig. 3b demonstrates TG and DTA curves of the glycolate $Ti_{0.95}Fe_{0.05}(OCH_2CH_2O)_{1.975}$ exposed for 2 hr in a helium atmosphere at 500 °C. The DTA curve exhibits an exothermal effect with a maximum at 363 °C, to which the mass loss of 17.95 % (w) corresponds. According to elemental analysis, the total amount of carbon in this sample is 18.06 % (w). Thus, by annealing in air the thermolysis products of $Ti_{1-x}Fe_x(OCH_2CH_2O)_{2-x/2}$, obtained by heating in a helium atmosphere, it is possible to register a certain amount of carbon in them. The quantity of chemically bonded carbon in these products depends on the temperature and the time of oxidizing annealing. This technique enables one to synthesize the iron- and carbon-doped titanium dioxide $Ti_{1-x}Fe_xO_{(2-x/2)-y}C_y$ with the anatase structure and to produce composites based thereon having an excess elemental carbon content.

It is known that doping of titanium dioxide with cations may lead not only to an increase in its liquid-medium photocatalytic activity in oxidation reactions of toxic and colored organic substances, but also to its bathochromic shift to the visible spectral region [3, 19, 22, 23, 25]. In the case of vanadium and carbon co-doping of the titania powder, the bathochromic shift in its catalytic activity may be extended to the blue light region for the samples of the composition $Ti_{0.50}Fe_{0.50}O_{2-y}C_y$ [22].

To evaluate the chemical stability of the doped catalysts during photocatalytic oxidation of hydroquinone, three consistent irradiation cycles of the same catalyst with the newly prepared solution were performed. Before each new cycle, the catalyst was washed with distilled water. These experiments indicated that the catalysts $Ti_{1-x}Fe_xO_{2-x/2}$ are chemically stable and do not

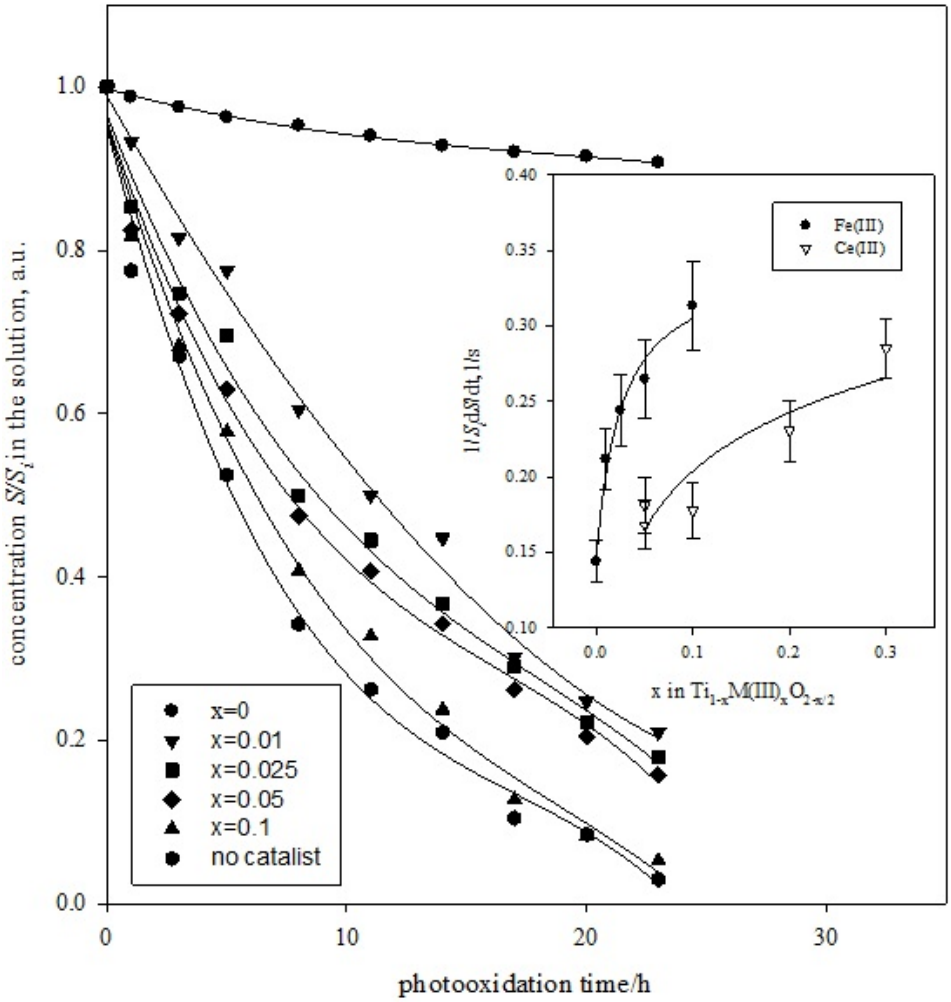


FIG. 4. The relative concentration of hydroquinone ($S/S_i$) versus the time of irradiation with ultraviolet light in the presence of $Ti_{1-x}Fe_xO_{2-x/2}$. In the inset the initial rate of hydroquinone photooxidation $1/S_i \cdot (dS/dt)_{t=0}$ versus the concentration ($x$) of M(III) atoms in the Ti(IV) oxide solid solution is depicted and lines on the graph show qualitative tendency of variation. Here $S$ and $S_i$ are current and initial concentration of HQ in solution, mM/l

change their chemical composition at least during three photo-oxidation cycles. Fig. 4 is a typical example of the experimental dependence of the related concentration of HQ ($S/S_i$) on their radiation time for a series of solid solutions $Ti_{1-x}Fe_xO_{2-x/2}$ ($x = 0.01$; 0.025; 0.05; 0.1).

The inset in Fig. 4 depicts the observed correlation of the initial $S/S_i$ (relative) rate of hydroquinone photooxidation on the concentration 'x' of dissolved in the titania catalyst metal M (M=Fe(III), Ce(III)). One can see that the initial rate of the photocatalytic reaction increases with the concentration of the dopant (Fig. 4).This implies that the rate of photooxidation at the initial stage of the process is a function of structural and energetic changes in the solid solution, which are due to doping of titania with M(III) cations.

### 3.2. Discussion and modeling

Doping is a key factor for fabricating light-sensitive photocatalysts with advanced properties. Though solid solution formation is one of the convenient ways for empirical photocatalysts 'tuning', no methodology is available to prove enhanced catalysis through titania doping [28]. One of the parameters, which allows estimating the above energetic effect of solid solution formation on the photocatalytic activity, is mixing enthalpy of the solid solution formation ($\Delta H_{mix}$) [29]. If so, we can expect a certain functional correlation between the terms $-\ 1/S_i \cdot (dS/dt)$ (or the energy of photooxidation of HQ by M-doped titania, $\Delta E_r \sim \ln[-1/S_i \cdot (dS/dt)]$) on one hand and $\Delta H_{mix}$ on the other hand.

In terms of the concept of regular solid solutions, which is a first approximation in the case of low levels of M ions solubility in titania, the mixing enthalpy $\Delta H_{mix}$ for the binary ionic crystal $\mathrm{Ti_{1-x}Fe_xO_{2-x/2}}$ [29, 30] is:

$$\Delta H_{mix} \sim c(1-x)x(\Delta R/R)^2, \tag{2}$$

where $R$ is the average M–O–M($Ti^{4+}$–$O^{2-}$–$Fe^{3+}$) distance in the solid solution estimated by using Vegard's rule in the form $R = R_{Ti^{4+}}(1-x) + R_{Fe^{3+}}x$, nm, and the term $\Delta R = R_{Fe^{3+}} - R_{Ti^{4+}}$ [30]. Here, $R_{Ti^{4+}} = (r_{Ti^{4+}} + r_{O^{2-}})$, $R_{Fe^{3+}} = (r_{Fe^{3+}} + r_{O^{2-}})$, and $r_{Ti^{4+}}, r_{Fe^{3+}}, r_{O^{2-}}$ are the ionic radii of the ions with the coordination number 6 [31], nm. '$c$' in (2) is the empiric coefficient, which depends on the iconicity of M–O bonds, on the coordination number of cations in the crystal, and on the Madelung constant [30]. The term $(1-x)x(\Delta R/R)^2$ in (2) is a semiempirical approximation of $\Delta H_{mix}$ values variation in our experiments since the substituting cations M in the solid solution $\mathrm{Ti_{1-x}M_xO_{2-x/2}}$ have the same charge end coordination. Comparison of the variation of the terms $\ln[-1/S_i \cdot (dS/dt)]$ and $(1-x)x(\Delta R/R)^2$ in a series of photocatalytic experiments with the catalysts $\mathrm{Ti_{1-x}M_xO_{2-x/2}}$, M=Fe(III), Ce(III), revealed a linear correlation between these variables in any of the considered series. This allows us to conclude that the mixing enthalpy $\Delta H_{mix}$ is one of the driving forces for the photooxidation of HQ in the solid solutions $\mathrm{Ti_{1-x}M_xO_{2-x/2}}$, in which M is not only Fe(III), Ce(III) (Fig. 5, curves 1,2), but also tricharged ions of Er, Tb, Eu, Nd, Sm (Fig. 5, curve 3). In accordance with the accepted semi-empiric approach, the general difference in the catalytic activity of different series of catalysts can be ascribed to the curvature of the correlation lines plotted in the coordinates $\ln[-1/S_i \cdot (dS/dt)]$ and $(1-x)x(\Delta R/R)^2$, Fig. 5. According to Fig. 5, the slope of the correlation line is a constant for a given solid solution of ion 'M' in the series $\mathrm{Ti_{1-x}M_xO_{2-x/2}}$ and it differs for different 'M' ions. For tricharged ions of REE, such as Er, Tb, Eu, Nd and Sm, the difference in the slopes is negligible, due to a small difference in their ionic radii and in the M–O distances of these ions in the corresponding solid solutions. This is why only one line describes the whole series with REE ions except for $\mathrm{Ti_{1-x}Ce_xO_{2-x/2}}$. For Ce(III), the value of the slope may be a relative measure of photocatalytic activity of the $\mathrm{Ti_{1-x}M_xO_{2-x/2}}$ solid solutions. As to the effect of mixing enthalpy on the initial rate of HQ photooxidation, Eq. (2), the difference in the activity in the series $\mathrm{Ti_{1-x}M_xO_{2-x/2}}$ with different M is due to the difference of the empiric coefficient $c$, which depends on the iconicity of M–O bonds, coordination number of cations in the crystal, and on the Madelung constant [30]. Observed linear correlation between variables $\ln[-1/S_i \cdot (dS/dt)]$ and $(1-x)x(\Delta R/R)^2$ in the series of the solid solutions is a direct energetic consequence of the formation of the solid solution by the catalyst. This is why the energy of the photocatalytic reaction is proportional to the mixing energy of the solid solution $\mathrm{Ti_{1-x}Fe_xO_{2-x/2}}$, $\Delta E_r \sim \Delta H_{mix}$. The difference in the activity of Fe(III)- and Ln(III)-doped catalysts may be attributed to the marked ability of Fe(III) to drastically increase the charge-carriers lifetime in titania [3]. Thus, the lifetime of the

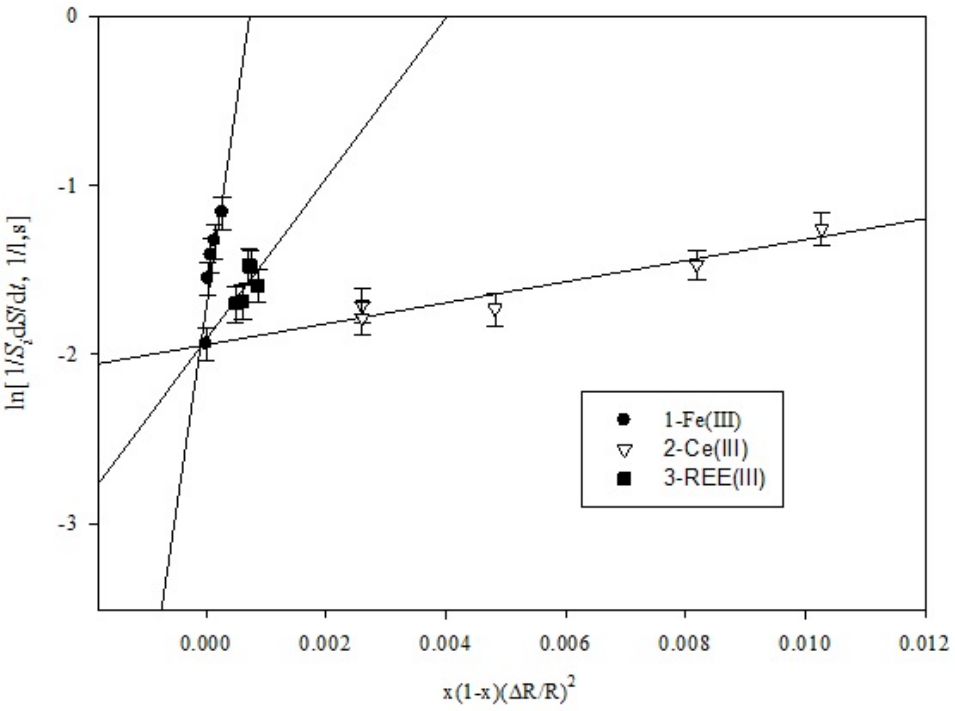


FIG. 5. The change in the initial rate of hydroquinone photo-oxidation $(\ln[1/S_i \cdot (dS/dt)_{t=0}])$ in the series of photocatalysts $Ti_{1-x}M_xO_{2-x/2}$, versus estimate of their solid solution mixing enthalpy $\Delta H_{mix} \sim (1-x)x(\Delta R/R)^2$; the dopants are Fe(III) for the $x = 0 - 0.0003$ (1), Ce(III) for $x = 0.05 - 1.00$ (2) and tricharged REE — Ce, Er, Tb, Eu, Nd, Sm for the $= 0.025$ (3)

carriers is connected with the mixing enthalpies of the solid solution formation for Fe(III) and for Ce(III), Er(III), Tb(III), Eu(III), Nd(III), Sm(III) in titania with fiber-like morphology.

The ability to create extended non-equilibrium solid solution by doping of titania with cations provides conditions for increasing the photocatalytic activity of the solid solution in the assigned spectral region. Conversely, in contrast to $Ti_{1-x}V_xO_{2-y}C_y$ and $Ti_{1-x}V_xO_2$ [22,23], the iron-doped quasi-one-dimensional titanium dioxide, like $Ti_{1-x}Ln_xO_{2-x/2}$ [24], does not activate the hydroquinone photooxidation process under blue light irradiation.

## 4. Conclusions

In summary, the studies performed show that with the use of $Ti_{1-x}Fe_x(OCH_2CH_2O)_{2-x/2}$ as a precursor, it is possible to obtain quasi-one-dimensional (1-D) solid solutions $Ti_{1-x}M_xO_{2-x/2}$ ($0 \leq x \leq 0.3$, M(III) = Fe, Ce, Er, Tb, Eu, Nd and Sm), which exhibit different photocatalytic activity in the HQ photooxidation under ultraviolet irradiation. The transformation of the precursor into oxide takes place in an isomorphous manner during heating both in air and in an inert atmosphere. In an inert gaseous atmosphere, the aggregates of $Ti_{1-x}Fe_x(OCH_2CH_2O)_{2-x/2}$ thermolysis products contain about 18 mass % carbon, which can be removed during subsequent aerobic annealing during the formation of anatase phases $Ti_{1-x}Fe_xO_{(2-x/2)-y}C_y$ and $Ti_{1-x}Fe_xO_{2-x/2}$. In the framework of ion-covalent binary solid solutions theory, a correlation is found between the energy of the photocatalytic reaction and the estimated mixing enthalpy of binary solid solutions formation. This approach may be useful for the semiempirical search for new ways of tuning the photocatalytic activity of binary solid solutions.

**Acknowledgments**

The work was supported by the RFBR (projects 12-03-00453-, 13-03-00265-a), RFBR-Urals (project 13-03-96061), the Presidium of RAS (projects 12-P-3-1915, 12-U-3-1009 and 12-T-3-1009), the Presidium of RAS (Urals Branch), the Science school (project SS-5669.2012.3).

## References

[1] Carp O., Huisman C.L., Reller A. Photoinduced reactivity of titanium dioxide. *Progress in Solid State Chemistry*, **32** (1–2), P. 33–177 (2004).

[2] Kubo W., Tatsuma T. Photocatalytic remote oxidation with various photocatalysts and enhancement of its activity. *J. Mater. Chem.*, **15** (30), P. 3104–3108 (2005).

[3] Banerjee S., Gopal J., et al. Physics and chemistry of photocatalytic titanium dioxide: Visualization of bactericidal activity using atomic force microscopy. *Current Sci.*, **90**, P. 1378 (2006).

[4] Egerton T., Kessel L., Tooley I.R., Wang L. Photogreying of $TiO_2$ nanoparticles. *J. Nanoparticle Res.*, **9** (2), P. 251–260 (2007).

[5] Pavasupree S., Jaturong J., Yoshikawa S. Hydrothermal synthesis, characterization, photocatalytic activity and dye-sensitized solar cell performance of mesoporous anatase $TiO_2$ nanopowders. *Mater. Res. Bull.*, **43**, P. 149–157 (2008).

[6] Balcerski W., Ryu S.Y., Hoffmann M.R. Gas-Phase Photodegradation of Decane and Methanol on $TiO_2$: Dynamic Surface Chemistry Characterized by Diffuse Reflectance FTIR. *Intern. J. Photoenergy*, Art. ID 964721 (2008).

[7] Kitano M., Tsujimaru K., Anpo M. Hydrogen Production Using Highly Active Titanium Oxide-based Photocatalysts. *Top. Catal.*, **49** (1–2), P. 4–17 (2008).

[8] Xia M., Zhang Q., et al. The large-scale synthesis of one-dimensional $TiO_2$ nanostructures using palladium as catalyst at low temperature. *Nanotechnology*, **20** (5), P. 055605 (2009).

[9] Kumar S.G., Devi L.G. Review on modified $TiO_2$ photocatalyst under UV/visible light: Selected Results and Related Mechanisms on interfacial charge carrier transfer dynamics. *J. Phys. Chem. A*, **115**, P. 13211–13241 (2011).

[10] Xiao Yutang, Xu ShuangShuang, Li ZhiHua, et al. Progress of applied research on $TiO_2$ photocatalysis-membrane separation coupling technology in water and wastewater treatments. *Chinese Sci. Bull.*, **55** (14), P. 1345–1353 (2010).

[11] Tueng S., Kanaev A., Chhor K. New homogeneously doped Fe(III)-$TiO_2$ photocatalyst for gaseous pollutant degradation. *Appl. Catal. A: General*, **399**, P. 191–197 (2011).

[12] Wang D., Yu R., Chen Y., et al. Photocatalysis property of needle-like $TiO_2$ prepared from a novel titanium glycolate precursor. *Solid State Ionics*, **172**, P. 101–104 (2004).

[13] Jiang X., Wang Y., Herricks T., Xia Y. Ethylene glycol-mediated synthesis of metal oxide nanowires. *J. Mater. Chem.*, **14** (4), P. 695–703 (2004).

[14] Krasilnikov V.N., Shtin .P., et al. Vanadyl and titanium glycolates as precursors for the preparation of oxide materials in the form of elongated microparticles and nanoparticles. *Nanotechnologies in Russia*, **3** (3), P. 106–111 (2008).

[15] Krasilnikov V.N., Shtin .P., et al. Synthesis and properties of titanium glycolate $Ti(OCH_2CH_2O)_2$. *Russian Journal of Inorganic Chemistry*, **53** (7), P. 1065–1069 (2008).

[16] Zaleska A. Doped-$TiO_2$: A Review. *Recent Patents Eng.*, **2** (3), P. 157–164 (2008).

[17] Nishijima K., Kamai T., et al. Photocatalytic Hydrogen or Oxygen Evolution from Water over S- or N-Doped $TiO_2$ under Visible Light. *Intern. J. Photoenergy*, Art. ID 173943 (2008).

[18] Su Y., Han S., et al. Preparation and visible-light-driven photoelectrocatalytic properties of boron-doped $TiO_2$ nanotubes. *Mater. Chem. Phys.*, **110** (2–3), P. 239–246 (2008).

[19] Carriazo J.G., Moreno M., Molina R.A., Moreno S. Incorporation of titanium and titanium-iron species inside a smectite-type mineral for photocatalysis. *Appl. Clay Sci.*, **50** (3), P. 401–408 (2010).

[20] Sun H., Wang S., et al. Halogen element modified titanium dioxide for visible light photocatalysis. *Chem. Eng. J.*, **162**, P. 437–447 (2010).

[21] Yang J., Chen D.-X., et al. Visible-light-driven photocatalytic degradation of microcystin-LR by Bi-doped $TiO_2$. *Res. Chem. Intermed.*, **37** (1), P. 47–60 (2011).

[22] Krasilnikov V.N., Shtin .P., et al. Synthesis and photocatalytic activity of $Ti_{1-x}V_xO_{2-y}C_y$ whiskers in hydroquinone oxidation in aqueous solutions. *Russian Journal of Inorganic Chemistry*, **58** (8), P. 1184–1194 (2010).

[23] Zainullina V.., Zhukov V.P., et al. Electronic structure and the optical and photocatalytic properties of anatase doped with vanadium and carbon. *Physics of Solid State*, **52**, P. 271–280 (2010).

[24] Krasilnikov V.N., Shtin .P., et al. Glycolate $Ti_{1-x}Ln_x(OCH_2CH_2O)_{2-x/2}$ as an efficient precursor for synthesis of titanium dioxide doped with lanthanides $Ti_{1-x}Ln_xO_{2-x/2}$. *Doklady Chemistry*, **437** (2), P. 112–115 (2011).

[25] Baklanova I. V., Krasil'nikov V. N., Perelyaeva L. A., Gyrdasova O. I. Stability of the anatase phase in nanodimensional titanium dioxide doped with europium(III), samarium(III), and iron(III). *Theoretical and Experimental Chemistry*, **47** (4), P. 215–218 (2011).

[26] Sathishkumar P., Anandan S., et al. Synthesis of Fe3+ doped $TiO_2$ photocatalysts for the visible assisted degradation of an azo dye. *Colloids and Surfaces. A: Physicochem. Eng. Aspects*, **375**, P. 231–236.

[27] Matsuura H., Miyazawa T. Infrared Spectra and Molecular Vibrations of Ethylene Glycol and Deuterated Derivatives. *Bull. Chem. Soc. Japan*, **40** (1), P. 85–94 (1967).

[28] Ohtani B. Photocatalysis A to Z-What we know and what we do not know in a scientific sense. *Journal of Photochemistry and Photobiology C: Photochemistry Reviews*, **11**, P. 157–178 (2010).

[29] Urusov V. S. Crystal Chemical and Energetic Characterization of Solid Solution. *Thermodynamic Data Advances in Physical Geochemistry*, **10**, P. 162–193 (1992).

[30] Urusov V.S. Comparison of Semi-Empirical and Ab Initio Calculations of the Mixing Properties of MO–M'O Solid Solutions. *Journal of Solid State Chemistry*, **153** (2), P. 357–364 (2000).

[31] Shannon R.D. Revised effective ionic radii and systematic studies of interatomic distances in halides and chalcogenides. *Acta Crystallogr. A*, **32**, P. 751–767 (1976).